Journal of Power Sources 203 (2012) 17–25

Contents lists available at SciVerse ScienceDirect

Journal of Power Sources

journal homepage: www.elsevier.com/locate/jpowsour

Facile synthesis of hollow spherical sandwich PtPd/C catalyst by electrostatic self-assembly in polyol solution for methanol electrooxidation

Yuan-Yuan Chu[a,b], Zhen-Bo Wang[a,*], Zheng-Zhi Jiang[a,b], Da-Ming Gu[b], Ge-Ping Yin[a]

[a] School of Chemical Engineering and Technology, Harbin Institute of Technology, No. 92 West-Da Zhi Street, Harbin 150001, China
[b] Department of Applied Chemistry, Harbin Institute of Technology, No. 92 West-Da Zhi Street, Harbin 150001, China

ARTICLE INFO

Article history:
Received 27 September 2011
Received in revised form 9 November 2011
Accepted 9 November 2011
Available online 18 November 2011

Keywords:
Direct methanol fuel cell
Microwave-assisted ethylene glycol process
Electrostatic self-assembly
Hollow spherical PtPd/C catalyst
Methanol electrooxidation

ABSTRACT

A novel PtPd/C catalyst with hollow spherical structure has been successfully prepared by electrostatic self-assembly one-step reductive route using sodium dodecyl sulfate as a capping and structure-directing agent in ethylene glycol solution by microwave-assisted process. The structure, composition, and morphology of as-prepared catalyst are characterized by X-ray diffraction, energy dispersive analysis of X-ray, scanning electron microscope, and transmission electron micrograph, respectively. The as-prepared PtPd/C catalyst has a novel hollow spherical sandwich structure with open porosity and integrity, which can prevent Pd metal from oxidation and dissolution, and enhance electrocatalytic activity and stability toward methanol electrooxidation in comparison with the solid solution PtPd/C alloy and Pt/C catalysts. The results of electrochemical measurement demonstrate the enhancement of the CO-tolerant ability of hollow spherical PtPd/C catalyst by the new insight into the mechanism that Pd can efficiently directly oxidize the poisoning intermediates from methanol electrooxidation, such as HCOOH, to CO_2, which promotes its catalytic efficiency and results in much higher electrocatalytic activity than Pt/C on a mass basis. Therefore, the effective and facile method to prepare PtPd/C catalyst with hollow spherical sandwich and porous structure and better catalytic performance is very important and desirable in direct methanol fuel cell applications.

1. Introduction

Direct methanol fuel cell (DMFC) has low toxicity, and high energy density (3800 kcal L^{-1}) compared to proton exchange membrane fuel cell (PEMFC) using hydrogen (658 kcal L^{-1}) as a fuel, which is an attractive option for portable power equipments [1,2], and its structure system design is very simple [3]. However, its cost and durability issues are two obstacles that limit and delay the large-scale commercialization of DMFC system. The main reason for DMFC anode with poor reaction activity is apparently the sluggish electrooxidation of adsorbed carbon monoxide, an intermediate of methanol oxidation [4], which reduces the cell performance even at low concentrations (<5 ppm) [5]. Many research efforts to weaken CO poisoning have been made through using additional elements to platinum such as Ru, Sn, and Ni [3,6–8]. In order to achieve high catalytic performance and reduce the loading of noble metal, some effective ways were adopted to prepare the catalysts with special nanostructures, such as core–shell and hollow metal nanostructure [9,10]. Liu et al. [11] successfully prepared PtMo alloy and MoOx@Pt core–shell nanoparticles (NPs) by a chemical co-reduction and sequential chemical reduction method, respectively. And both catalysts showed remarkably high CO tolerance compared to the commercialized E-TEK PtRu alloy and Pt catalysts. The well-dispersed Ni@Pd core–shell nanoparticles supported on multi-wall carbon nanotubes have been successfully synthesized by Zhao et al. [12], which showed apparently the enhancement of electrocatalytic activity and stability for methanol oxidation in alkaline media. Zhong et al. [13] investigated the nano-structural relationships between the novel core–shell Au@Pt, Pt@Au, and Fe_3O_4@Au nanocatalysts (NPs) and methanol oxidation reaction (MOR) and oxygen reduction reaction (ORR). Their research results showed that the increasing of kinetic current and the positive-shift of the reduction potential followed in the order of Au < Pt@Au < Au@Pt < Fe_3O_4@Au@Pt < Pt for ORR and the highest activity of Fe_3O_4@Au@Pt catalyst for MOR was exhibited, indicating that its electrocatalytic activities were nearly determined by the nanoscale spatial arrangement of the metals, and the oxide core also played an important role in that. Chen et al. [14] introduced one-step chemical synthesis of Co–Pt hollow spherical catalyst with changeable compositions. Investigations showed that their electrocatalytic activity toward methanol oxidation was evidently enhanced in comparison with Pt nanoparticles. Teng et al. [15] prepared novel carbon nanocages (CNCs) with a special hollow structure with graphitic shells as a

* Corresponding author. Tel.: +86 451 86417853; fax: +86 451 86418616.
E-mail address: wangzhenbo1008@yahoo.com.cn (Z.-B. Wang).

0378-7753/$ – see front matter © 2011 Elsevier B.V. All rights reserved.
doi:10.1016/j.jpowsour.2011.11.025

catalyst support. The catalyst exhibited excellent performance for PEMFC.

Most researchers focused on the investigation of catalytic performance of Pd-based catalysts for methanol or ethanol electrooxidation [16–18] in alkaline media due to the fact that they only have catalytic activity for methanol or ethanol in alkaline media rather than in acid media. While Pd-alone is used as a co-catalyst in acid media, a new mechanism on methanol electrooxidation on PtPd catalyst is put forward in this work. In addition, many efforts have been devoted to the metal nanostructures investigations deriving from their unique catalytic properties [19] in order to mitigate the "poisoning effect" of catalyst from CO-like species produced during electrochemical process.

In present paper, a hollow spherical sandwich PtPd/C catalyst has been prepared by microwave-assisted polyol process. And an anionic surfactant sodium dodecyl sulfate (SDS) was used as a capping and structure-directing agent [14]. Various techniques have been used to characterize the formation of hollow spherical sandwich PtPd/C alloy, including X-ray diffraction (XRD), energy dispersive analysis of X-ray (EDAX), scanning electron microscope (SEM), transmission electron micrograph (TEM), and conventional electrochemical methods. The as-prepared PtPd/C catalyst exhibits the enhancement of electrocatalytic activity by the change of reaction mechanism of methanol electrooxidation and stability due to the novel hollow spherical sandwich structure compared with the solid solution PtPd/C alloy and Pt/C catalysts, which is very important and desirable for an anode electrocatalyst of DMFC.

2. Experimental

2.1. Preparation of hollow spherical sandwich PtPd/C catalyst by microwave-assisted polyol process

Briefly, $PdCl_2$ was firstly dissolved in ethylene glycol (EG) solution, then sodium dodecyl sulfate (SDS) and H_2PtCl_6 were added to form a homogeneous solution under continuous stirring, The pH value of the ink was adjusted to 9 by adding 1 mol L^{-1} NaOH-EG solution drop by drop, which measured by the pHS-32 meter. And then the beaker was placed the center of a microwave oven (2450 MHz, 800 W) and argon gas was feed into the ink for 15 min to remove oxygen for continuous microwave heating (IMH) for 50 s. After cooling down to room temperature, the dispersed carbon ink was added into the above solution with stirring overnight. The slurry was allowed continuous stirring at room temperature, and then 0.1 mol L^{-1} HNO_3 was added into the cooled mixture to adjust pH value of the solution to about 4. The mixture was kept stirring for 3 h and then the product was washed repeatedly with ultrapure water (18.2 MΩ cm) until no Cl^- ions were detected. The as-prepared catalyst was dried for 3 h at 80 °C and then stored in a vacuum vessel. All chemicals used were of analytical grade. For comparison, the solid solution PtPd/C alloy and Pt/C catalysts were also obtained by the similar preparation process without the addition of SDS.

2.1.1. Preparation of working electrode

The ultrasonically re-dispersed catalyst suspension (5 μL) was spread by pipette onto the glassy carbon disk substrate. The subsequent evaporation of solvent leads to the formation of the deposited catalyst layer (28 $\mu g_{metal}\ cm^{-2}$), onto which 5 μL of a dilute aqueous Nafion® solution (5 wt.% solution in a mixture of lower aliphatic alcohols and ultrapure water) was applied. The resulting Nafion® film with a thickness less than 0.2 μm had the sufficient strength to keep carbon particles permanently on the glassy carbon electrode without producing significant film diffusion resistances [20]. The glassy carbon working electrode with 3 mm of diameter and 0.0706 cm^2 of electrode area was polished with 0.05 μm alumina to a mirror finish before being used as the substrate for carbon-supported catalyst.

2.1.2. Electrochemical measurements

Electrochemical measurements were carried out in a conventional sealed three-electrode electrochemical cell at 25 °C, with the glassy carbon disk electrode made in the above mentioned procedure as the working electrode and a piece of Pt foil (1 cm^2) as the counter electrode. The reference electrode was a reversible hydrogen electrode (RHE) with its solution connected to the working electrode chamber by a Luggin capillary whose tip was placed appropriately close to the working electrode. All chemicals used were of analytical grade, and solutions were prepared with ultrapure water (MilliQ, Millipore, 18.2 MΩ cm). The solution of 0.5 mol L^{-1} H_2SO_4 containing 0.5 mol L^{-1} CH_3OH was kept on constantly stirring and purging with ultrapure argon gas. The cyclic voltammograms (CV) were recorded within a potential range from 0.05 V to 1.2 V. The amperomeric *i–t* curves were plotted with CHI650A electrochemical analysis instrument controlled by an IBM PC. In order to get rid of the possible contaminations caused by Nafion® film, the working electrode was treated by continuously cycling at 0.05 V s^{-1} until a stable response was obtained before the measurement curves were recorded. Fresh electrolyte solution was used for each time electrochemical measurement in order to ensure repeated results. All potentials are reported vs. RHE in this paper.

2.2. Characterization of physical properties

2.2.1. X-ray diffraction (XRD)

XRD analysis of catalyst was carried out with the diffractometer (D/max-rB-Rigaku) using a Cu Ka X-ray source operating at 45 kV and 100 mA, scanning at a rate of 4° min^{-1} with an angular resolution of 0.05° of the 2θ scan to get the XRD pattern.

2.2.2. Scanning electron microscopy (SEM) and energy dispersive analysis of X-ray (EDAX)

For a rapid SEM and EDAX analysis of chemical composition, morphology and microstructure, the Hitachi-S-4700 analyzer was coupled to a scanning electron microscope (SEM, Hitachi Ltd., S-4700), with the incident electron beam energies ranging from 3 to 30 keV, which impinges the sample surface from the normal angle. The measurement time was 100 s, and the EDAX spectra were obtained by using the ZAF correction, and the samples were supported on the aluminum foil in order to eliminate the influence of the conductive carbon tape.

2.2.3. Transmission electron microscopy (TEM) with high resolution (HRTEM), high-angle annular dark field (HAADF), and the energy-dispersive X-ray spectroscopy (EDS)

TEM, HRTEM, HAADF images and EDS for the catalyst samples were taken by a field emission transmission electron microscope (TEM, TECNAI G2 F30) with a point resolution of 0.20 nm. Before taking the electron micrographs, the samples were finely ground and ultrasonically dispersed in ethanol, and a drop of the resultant dispersion was deposited and dried on a standard copper grid coated with carbon film. The applied voltage was 300 kV.

2.2.4. X-ray photoelectron spectrometry (XPS)

X-ray photoelectron spectroscopy (XPS) analysis was performed to determine the chemical state of Pt and Ru with a physical electronics PHI model 5700 instrument. The Al X-ray source operated at 250 W. The sample to analyzer take off angle was 45°. Survey spectra were collected at pass energy (PE) of 187.85 eV over a binding energy range from 0 eV to 1300 eV. High binding energy resolution

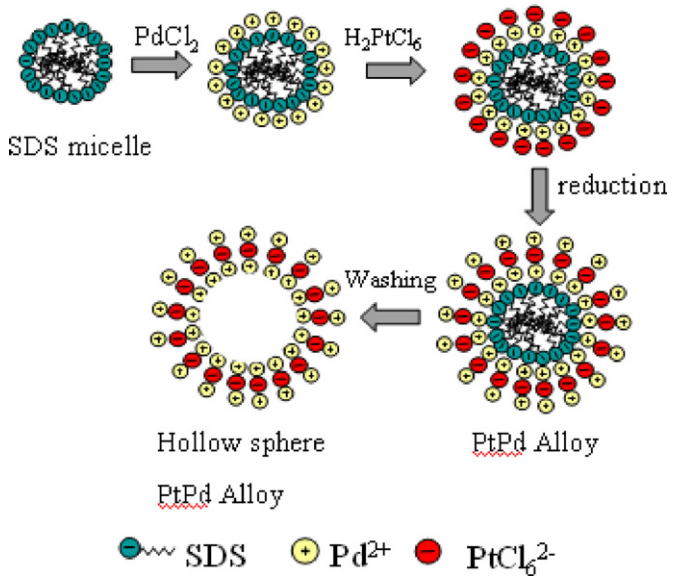

Fig. 1. Schematic diagram of formation process of hollow spherical PtPd catalyst.

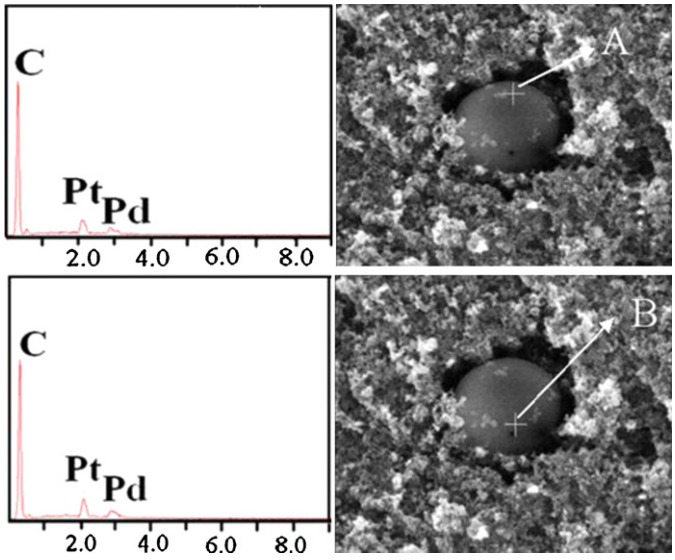

Fig. 2. EDAX spectra of hollow spherical PtPd/C catalyst at different spots on a hollow sphere.

multiplex data for the individual elements were collected at a PE of 29.55 eV. The C 1s electron binding energy was referenced at 284.6 eV, and a nonlinear least-squares curve-fitting program was employed with a Gaussian–Lorentzian production function [21,22]. During all XPS experiments, the pressure inside the vacuum system was maintained at 1×10^{-9} Torr. Before analysis above, all the samples were dried under vacuum at 80 °C overnight.

3. Results and discussion

3.1. Formation mechanism of hollow spherical sandwich PtPd/C alloy catalyst

Based on the experimental process and data, the possible formation mechanism of hollow spherical sandwich PtPd/C catalyst is proposed here as shown in Fig. 1. In the reacting mixture, the SDS is very necessary, which may form micelles as reported in the literature [12]. It is well known that the SDS is an anionic surfactant and has weakly negative charge, which is regarded as a template in the self-assembly process, leading to the self-assembly of the positive charge Pd^{2+} precursors on the SDS micelles surface, followed by the subsequent self-assembly of negative charge $[PtCl_4]^{2-}$ precursors. In the presence of reducing process, PtPd nanoparticles were formed in the initial period, and then supported on XC-72 carbon black under vigorous stirring. The SDS micelles were removed with ethanol and water for several times, and the hollow spherical sandwich PtPd/C catalyst was synthesized in EG solution.

3.2. Characterization of hollow spherical sandwich PtPd/C catalyst

The typical EDAX spectra of the hollow spherical sandwich PtPd/C catalyst are presented in Fig. 2. It can be seen that their metal mass percentage at the different spots of A and B on a hollow sphere are similar. Their compositions are listed in Table 1, which are coincided with the theoretical value of total metal loading of 20% and Pt to Pd atomic ratio of 1:1. The experimental data show that the hollow spherical PtPd/C catalyst has a uniform surface composition. The solid solution PtPd/C catalyst also has the similar metal mass percentage and the composition of Pt to Pd atomic ratio is 1:1 as expected, which is not listed here.

Table 1
Comparison of metal loading, Pt to Pd atomic ratio at different spots on a hollow sphere in hollow spherical PtPd/C catalyst.

Different spots on hollow spherical PtPd/C catalyst	C (wt.%)	Pt (wt.%)	Pd (wt.%)	Atomic ratio of Pt to Pd
A	81.11	13.01	6.67	1.01:0.95
B	81.31	12.30	6.39	0.91:0.87

The XRD patterns of hollow spherical sandwich PtPd/C and solid solution PtPd/C catalysts are presented in Fig. 3. XRD pattern of the Pt/C catalyst also is listed for comparison. The diffraction peak at $2\theta < 30°$ is attributed to the XC-72 carbon support. For Pt/C catalyst, these peaks are clearly visible at 2θ values of about 39.7°, 46.2°, 67.4°, and 81.2°, respectively. For PtPd/C catalysts, the diffraction peaks located at 2θ values of about 39.7°, 46.1°, 67.6°, 81.4°, and 85.9°, are characteristic of face-centered cubic (fcc) structure, corresponding to the planes (1 1 1), (2 0 0), (2 2 0), (3 1 1), and (2 2 2), respectively. Since the atom sizes of Pt and Pd are similar and their crystal structures are the same, they have similar diffraction peaks

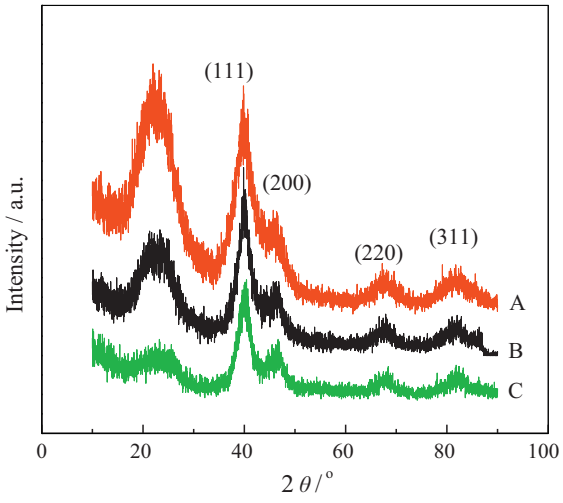

Fig. 3. XRD patterns of Pt/C (A), hollow spherical PtPd/C (B), and solid solution PtPd/C (C) catalysts.

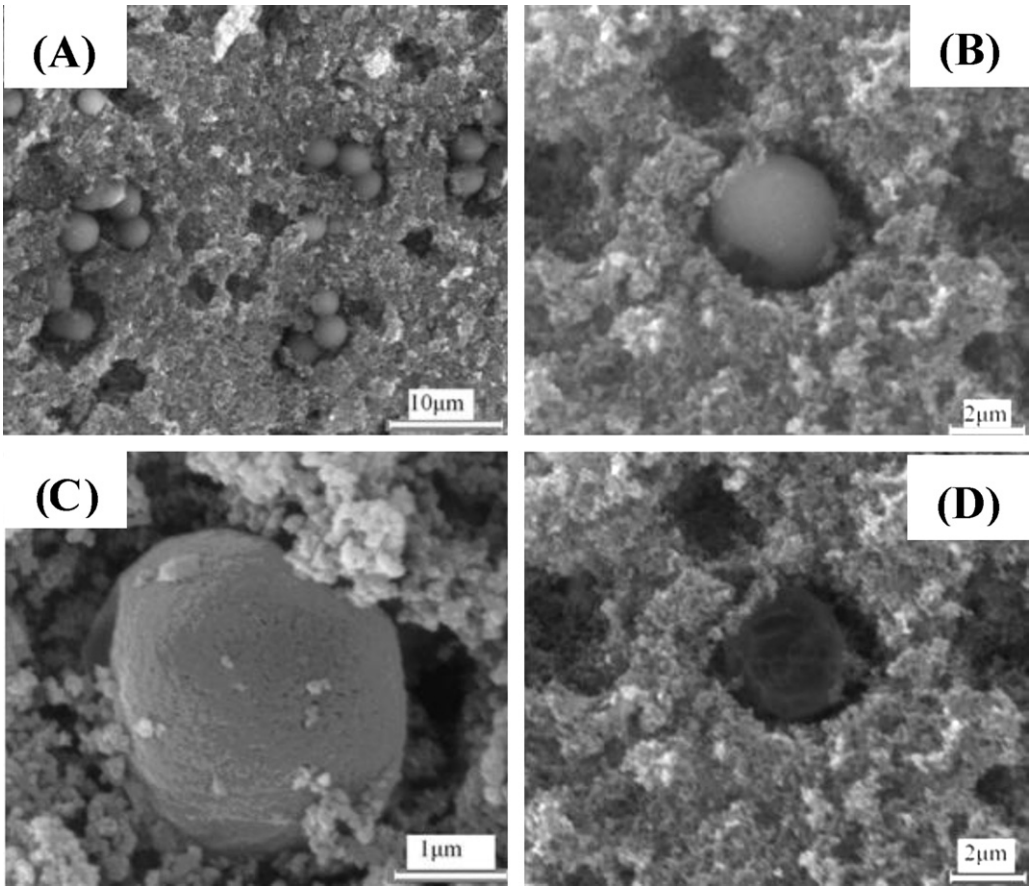

Fig. 4. SEM images of hollow spherical PtPd/C catalyst.

[23]. The lattice parameters of the hollow spherical sandwich and solid solution PtPd/C catalysts are 0.392 nm, calculated according to Vegard's law [24], which is slightly smaller than that of Pt/C catalyst (0.394 nm), indicating the incorporation of Pt and Pd atoms in the same lattice to form PtPd alloy.

Fig. 4 shows the SEM images of hollow spherical PtPd/C catalyst. It can be clearly seen from Fig. 4(A) that the as-prepared PtPd/C catalyst is composed of many balls with average diameter of 3–4 μm and they look like tiny eggs in a nest. Fig. 4(C) shows that the surface of the ball is open porous with excellent structure continuity and integrity, which results from the self-assembly between Pt layer and Pd layer due to electrostatic function of SDS. Fig. 4(B) and (D) is the same sphere before and after SEM scanning shooting with the electron beam energy of 15 kV. The sphere drastically contrasts after electron beam shooting, which provides convincingly evidence that the spherical PtPd/C microparticle is a hollow structure. Compared to the results of XRD and TEM below, it may be concluded that the as-prepared PtPd/C catalyst is made of a number of PtPd nanoparticles by electrostatic self-assembly of multi-layers with hollow structure.

Fig. 5 shows the TEM images of the hollow sphere PtPd/C (A and B) and solid solution PtPd/C catalysts (C and D). The hollow spherical PtPd/C catalyst in Fig. 5(A) shows the sphere clusters morphology with the discontinuous peripheral alloy in dark color and the flocculent holes in light color. This is absolutely different from the solid solution PtPd/C catalyst in Fig. 5(C), which are desultory and dark, indicating further that the PtPd/C catalyst prepared by the addition of SDS is a hollow and porous structure, which is consistent with the results obtained from SEM images. The diameter of hollow ball of PtPd catalyst estimated from TEM image is also in good agreement with that obtained from SEM images above, in scale of 2 μm. Furthermore, the particles of the PtPd/C catalyst prepared with the addition of SDS as shown in Fig. 5(B) is relatively tint and their array is a bit orderliness as presented in white lines, indicating again that the PtPd/C catalyst with the hollow spherical sandwich structure is formed. It can be seen that both catalysts have the uniform dispersion with small particle size about 2.3 and 2.4 nm according to the particle size distribution histograms inserted. Finally, the HADDF-STEM images in Fig. 5(E) and (F) depict the fine structure of catalysts. Both compose of PtPd particles due to no evident contrast variations between Pt and lighter element Pd. Herein, the square regions in Fig. 5(E) prove again the hollow sphere PtPd/C structure, which are different from the PtPd/C catalyst in Fig. 5(F).

XPS wide scans and XPS core level spectra of hollow spherical PtPd/C and solid solution PtPd/C catalysts are shown to provide additional information about their surface structure in Fig. 6(A) and (B), respectively. Carbon, platinum, and palladium are revealed in two samples, the atomic ratios of Pt and Pd are 1.08 and 0.92 for hollow spherical PtPd/C and solid solution PtPd/C catalysts, respectively. Detailed experimental data are listed in Table 2. They are very close to the theoretical estimation of 1:1. Comparison of binding energies and surface compositions from deconvolution of XPS spectra for hollow spherical PtPd/C and solid solution PtPd/C

Table 2
Comparison of atomic ratio of XPS spectra for hollow spherical PtPd/C and solid solution PtPd/C catalysts.

Catalyst	C 1s	Pt 4f	Pd 3d
Hollow spherical PtPd/C alloy	95.80	2.19	2.01
Solid solution PtPd/C alloy	95.66	2.08	2.26

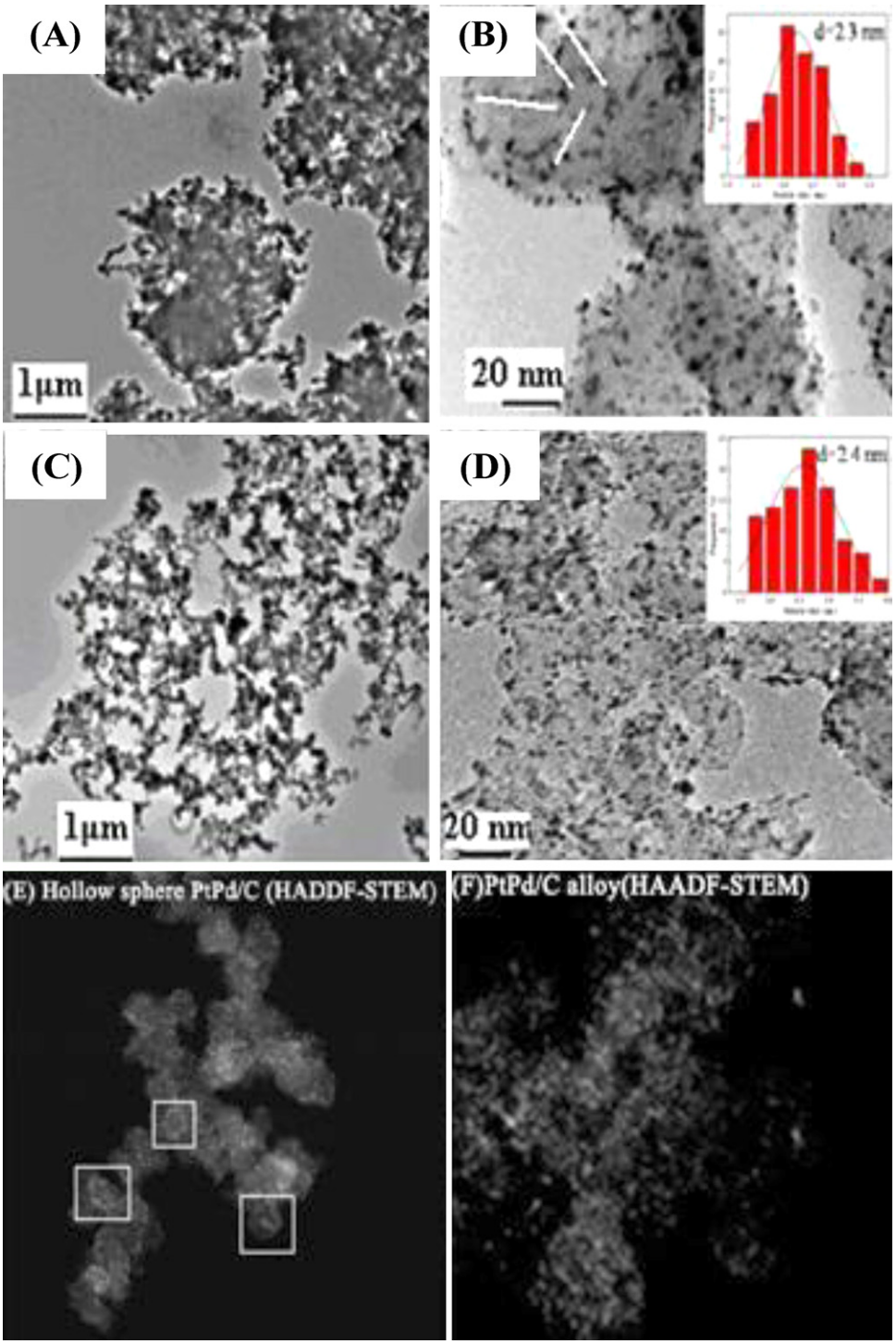

Fig. 5. TEM images of hollow spherical PtPd/C (A and B) and solid solution PtPd/C catalysts (C and D).

catalysts are presented in Table 3, where the Pt(0) amount is nearly equal in both PtPd/C catalysts, but metals compounds were greatly reduced. However the content of Pd(Π) in solid solution PtPd/C catalyst is nearly two times as much as that in hollow spherical PtPd/C one, indicating the hollow spherical PtPd/C catalyst with sandwich structure may efficiently prevent from Pd oxidation because of the cover by Pt layer, avoiding Pd dissolution in working conditions. This is its unique advantage compared to solid solution structure for DMFC and supported by high-resolution energy dispersive spectroscopy (EDS) in Fig. 7. It is obvious that the atomic ratio of Pt and Pd are both nearly theoretical value of 1:1 before aging test (1000 continuous CV cycling as below), but the varied to 7:1 and 10:1 for hollow spherical PtPd/C and solid solution PtPd/C catalysts, respectively, further proving that the sandwich structure of the former can effectively inhibit the Pd dissolution loss. The other reason may be that the hollow spherical PtPd/C catalyst is more homogeneous, with extensive Pt–Pd interactions to stabilize the Pd against dissolution, as opposed to more amorphous Pd–Pt bulk alloys where high Pd concentration regions will be more prone to dissolution.

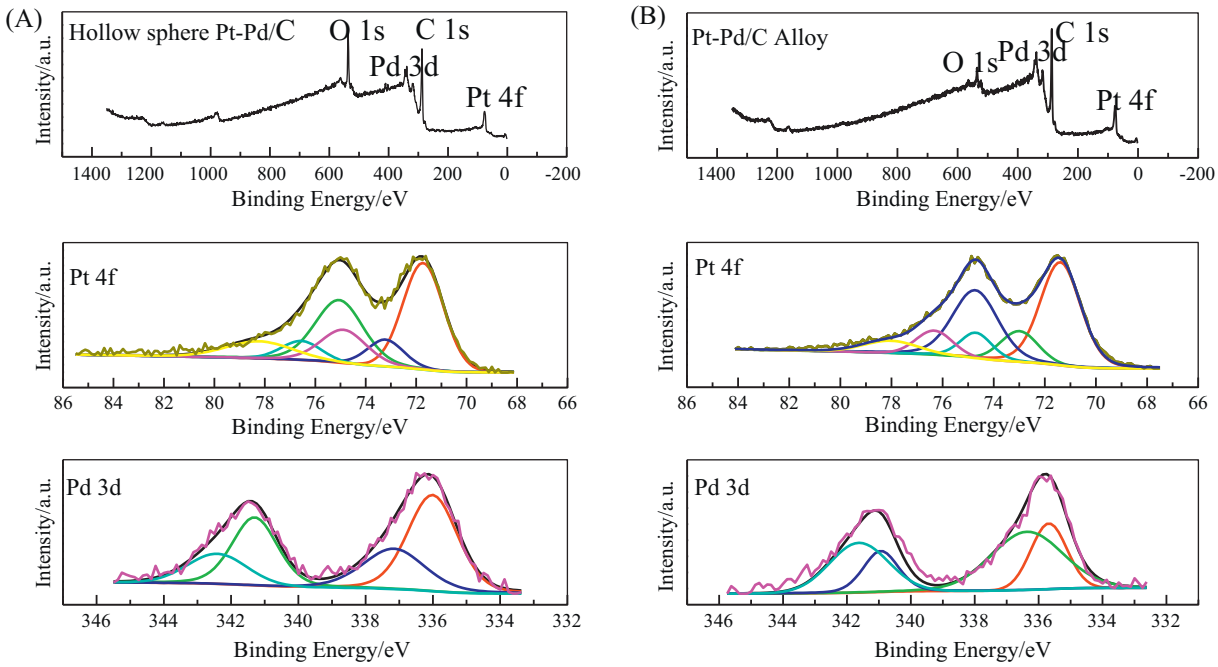

Fig. 6. XPS wide scan spectra and core level spectra of hollow spherical PtPd/C (A) and solid solution PtPd/C (B) catalysts.

Moreover, high resolution transmission electron microscopy (HRTEM) images and the inserted electron diffraction patterns of both catalysts in Fig. 8 show that the crystallite sizes increase after aging test. With the benefit of sandwich structure, the particle size of hollow spherical PtPd/C catalyst increase from 2.3 to 2.9 nm, compared to 2.4–3.1 nm for solid solution PtPd/C alloy (see Fig. 9).

3.3. Electrochemical characterization

Fig. 10(A) exhibits the cyclic voltammograms (CVs) of hollow spherical PtPd/C, solid solution PtPd/C, and Pt/C catalysts in an Ar-saturated solution of 0.5 mol L^{-1} H_2SO_4 containing 0.5 mol L^{-1} CH_3OH at a scanning rate of 50 mV s^{-1} at 25 °C. A significant enhancement of the mass activity and a negative shift of oxidation

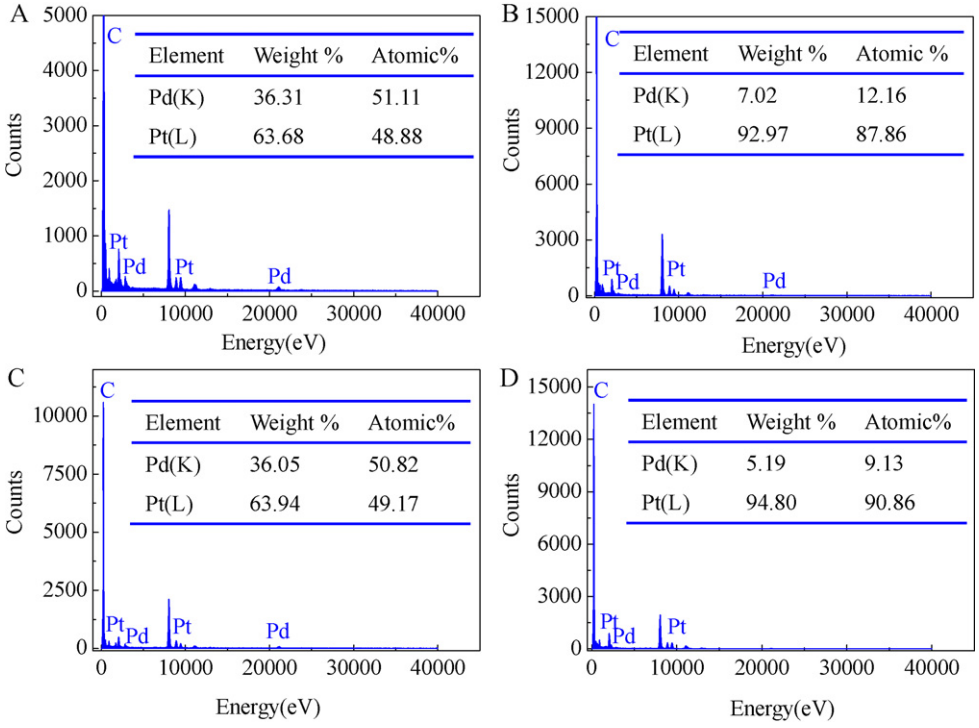

Fig. 7. EDS analysis of hollow spherical PtPd/C before (A) and after aging test (B) and solid solution PtPd/C catalysts (C and D).

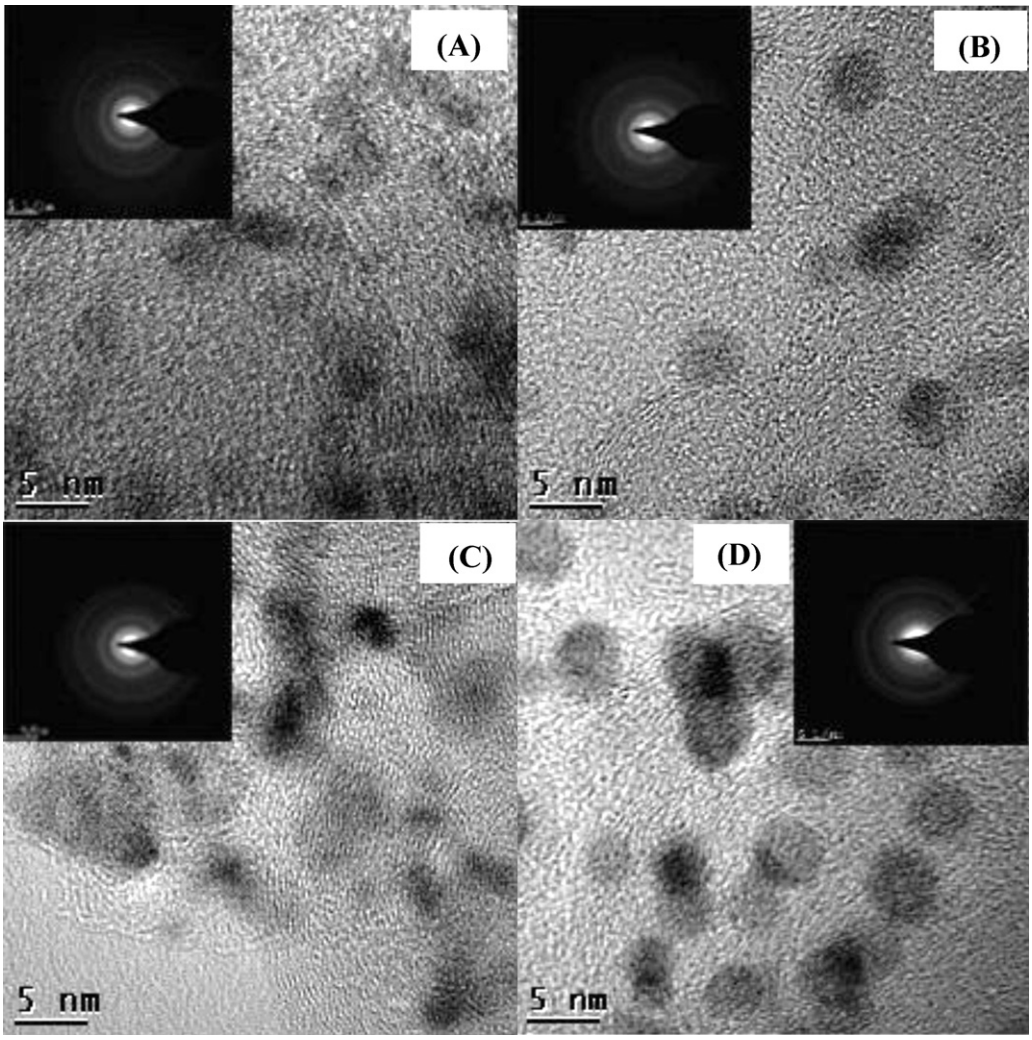

Fig. 8. HRTEM of hollow spherical PtPd/C before (A) and after aging test (B) and solid solution PtPd/C catalysts (C and D).

peak can be observed on hollow spherical PtPd/C and solid solution PtPd/C catalysts. Most possible reason is due to the addition of Pd element, as well as the particular structure and surface porosity in hollow spherical PtPd/C catalyst. In addition, the ratio of forward oxidation current peak (i_f) and the backward current peak (i_b), i_f/i_b, is an important index used to evaluate the catalyst tolerance to the poisoning species [25–28]. As shown in Fig. 10(A), the i_f/i_b ratios of the hollow spherical PtPd/C and the solid solution PtPd/C catalysts

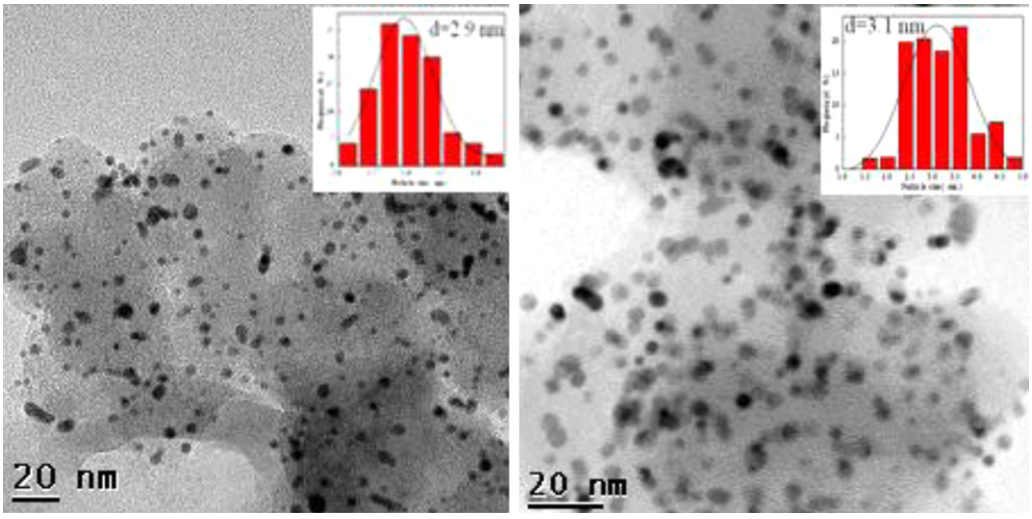

Fig. 9. TEM images of hollow spherical PtPd/C (A) and solid solution PtPd/C (B) after aging test.

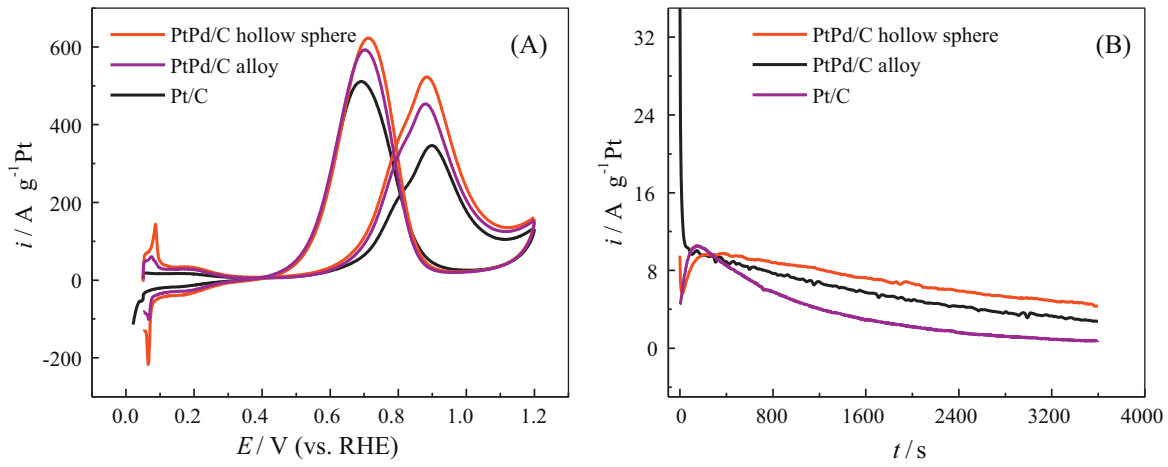

Fig. 10. Cyclic voltammograms (A) and amperomeric *i–t* (B) curves of hollow spherical PtPd/C, solid solution PtPd/C, and Pt/C catalysts in an Ar-saturated solution of 0.5 mol L^{-1} H_2SO_4 containing 0.5 mol L^{-1} CH_3OH at a scanning rate of 50 mV s^{-1} at 25 °C.

are 0.85 and 0.76, respectively, which are evidently higher than that of Pt/C one (0.66), indicating that hollow spherical PtPd/C catalyst has the better anti-poisoning ability. One more evidence could be found in the amperomeric *i–t* curves at a constant potential of 0.6 V (vs. RHE) in Fig. 10(B) that their catalytic activity follow in order of hollow spherical PtPd/C > solid solution PtPd/C alloy > Pt/C catalyst. It may be concluded that the high electrocatalytic activity of PtPd/C catalysts observed above can probably be ascribed to two major factors: (I) the hollow spherical PtPd/C catalyst with rough and porous structure may provide higher electrochemical active surface area, leading to higher electrocatalytic activity, as well as provide facile way for fuel transition; (II) adding Pd into catalyst can help to overcome CO-poisoning effect and/or efficiently directly oxidized the HCOOH and/or CO_{ads} species strongly adsorbed on the Pt surface, produced from step 1, 2, and 3, to CO_2 as step 4 below, which release the active sites and/or change the path of methanol electrooxidation by the addition of Pd, leading to excellent CO tolerance and higher electrocatalytic activity of the catalyst for DMFC [29].

Table 3
Comparison of binding energies and surface compositions from deconvolution of XPS spectra for hollow spherical PtPd/C and solid solution PtPd/C catalysts.

Catalyst	Peak	Binding energy (eV)	Species	Relative ratio (%)[a]
Hollow spherical PtPd/C alloy	Pt_{4f}	71.7	Pt metal	35.14
		75.0	Pt metal	26.32
		73.2	PtO	8.64
		76.5	PtO	6.48
		74.9	PtO_2	12.30
		78.2	PtO_2	10.03
	Pd_{3d}	336.0	Pd metal	38.00
		341.3	Pd metal	25.85
		337.2	PdO	21.22
		342.4	PdO	14.13
Solid solution PtPd/C alloy	Pt_{4f}	71.7	Pt metal	39.24
		75.0	Pt metal	29.41
		73.2	PtO	10.17
		76.5	PtO	7.63
		74.9	PtO_2	7.76
		78.2	PtO_2	5.79
	Pd_{3d}	336.0	Pd metal	21.04
		341.3	Pd metal	13.99
		337.2	PdO	38.96

[a] Relative concentrations are equal to the corresponding, deconvoluted peak areas divided by the total XPS area extracted from the experimental XPS core level regions of either Pt 4f or Pd 3d.

The electrocatalytic cycling stability of hollow spherical PtPd/C, solid solution PtPd/C, and Pt/C catalysts is compared in Fig. 11(A) with the continued cyclic voltammograms cycles and their peak current densities are presented in Fig. 11(B). The loss of electrocatalytic activity for hollow spherical PtPd/C is 20%, lower than 22% and 25% for PtPd/C and Pt/C catalysts, respectively. The former has the weak decline tendency after 1000 continuous CV cycling. The reason is that Pd may weaken the poisoning effect of Pt catalyst and the hollow spherical sandwich PtPd/C can efficiently inhibit Pd oxidation and dissolution, which can improve its durability. Hence, the hollow spherical sandwich PtPd/C catalyst has the high development potential for methanol electrooxidation.

The reasons that favor the choice of PtPd alloy system include: (I) Pd is inert in acid media and its surface is in favor of the reductive deposition of Pt [30,31]. (II) The reductive potential of Pd is similar with Pt, which facilities the formation of PtPd alloy by co-reduction reaction. (III) Pd can overcome the CO-poisoning effect in DMFC [29] and directly oxidize HCOOH to CO_2, which are favored by the new insight into the mechanism of methanol electrooxidation on PtPd catalyst, explained by the following pathway:

Methanol dehydrogenation producing poisoning intermediate:

$$CH_3OH \rightarrow CH_2OH \rightarrow CHOH \rightarrow COH \quad (1)$$

Poisoning intermediate oxidation producing HCOOH and CO_{ads}:

$$CHHO \rightarrow HCOOH \quad (2)$$

$$COH \rightarrow CO_{ads} \quad (3)$$

HCOOH oxidation on Pd catalyst directly producing CO_2 [32]:

$$HCOOH \rightarrow CO_2 + H^+ + e^- \quad (4)$$

HCOOH oxidation to COOH, further to CO_2:

$$HCOOH \rightarrow COOH \rightarrow CO_2 \quad (5)$$

The possible reason for the unexpectedly high activity for methanol electrooxidation on the PtPd/C hollow spherical catalyst is that Pd may efficiently oxidize the HCOOH and/or CO_{ads} poisoning small molecule produced from steps 2 and 3, where HCOOH is directly oxidized to CO_2 [33] as step 4, suppressing the step 5, namely, changing the path and mechanism of methanol electrooxidation. The bimetallic PtPd/C catalyst has demonstrated excellent CO tolerance and high electrocatalytic activity. (IV) Pd is less expensive than Pt, and development of low Pt content catalyst may

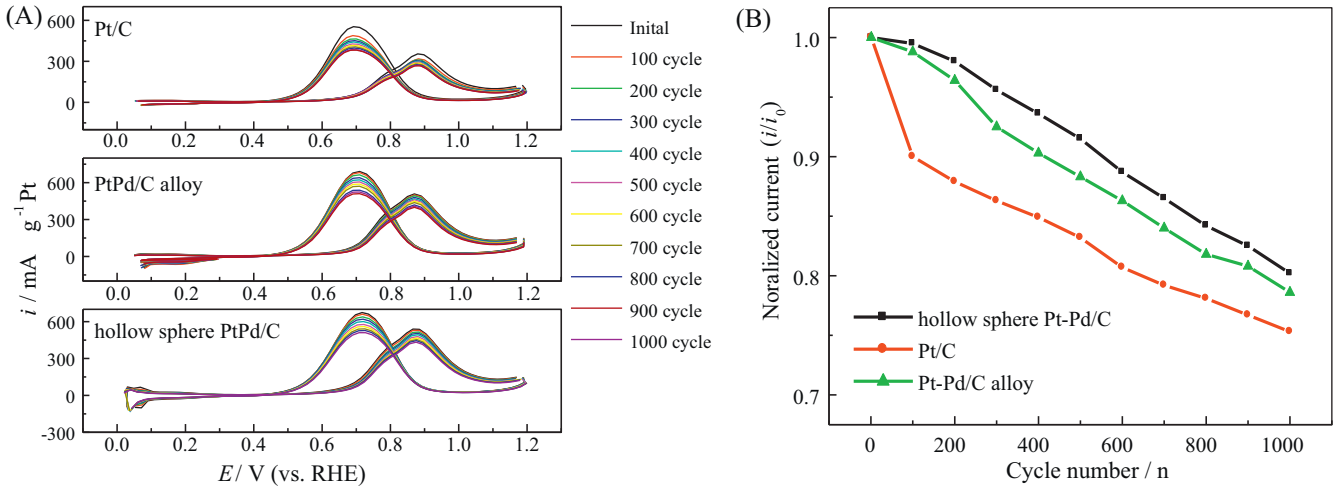

Fig. 11. (A) Continued cyclic voltammograms cycles (1000 cycles) of methanol electrooxidation in an Ar-saturated solution of 0.5 mol L^{-1} CH_3OH and 0.5 mol L^{-1} H_2SO_4 at a scanning rate of 50 mV s^{-1} at 25 °C on hollow spherical PtPd/C, solid solution PtPd/C, and Pt/C catalysts. (B) The normalized peak current plots for electrocatalytic cycling stability of hollow spherical PtPd/C, solid solution PtPd/C, and Pt/C catalysts (the data were normalized to the peak current of steady-state current).

improve utilization of Pt catalyst and thereby reduce the cost of DMFC and accelerate its commercialization.

4. Conclusions

In summary, we have successfully synthesized a hollow spherical sandwich PtPd/C catalyst by facile synthesis method in ethylene glycol solution by microwave-assisted process. The hollow spherical structure with Pd layer covered by Pt one, which may availably prevent Pd from oxidation and dissolution, enhance electrocatalytic activity and stabilize toward methanol electrooxidation in comparison with the solid solution PtPd/C and Pt/C catalysts. Its improvement of performance in this report is important for the understanding of HCOOH and/or CO_{ads} species directly oxidation to CO_2 on Pd sites, which plays very important role in enhancing the activity and CO-tolerance ability of catalyst. Considering the application of binary metal nanoparticles in other catalytic systems, it is expected this work may also find applications beyond DMFC.

Acknowledgements

This research is financially supported by the Science and Technology Ministry of China (863 program Grant No. 2009AA05Z111), the National Natural Science Foundation of China (Grant No. 20606007), the Scientific Research Foundation for the Returned Overseas Chinese Scholars, State Education Ministry (2008).

References

[1] H. Rivera, J.S. Lawton, D.E. Budil, E.S. Smotkin, J. Phys. Chem. B 112 (2008) 8458–8542.
[2] B. Gurau, E.S. Smotkin, J. Power Sources 112 (2002) 339–352.
[3] Z.B. Wang, G.P. Yin, Y.Y. Shao, B.Q. Yang, P.F. Shi, P.X. Feng, J. Power Sources 165 (2007) 9–15.
[4] M.A. Scibioh, S.K. Kim, E.A. Cho, T.-H. Lim, S.A. Hong, H.Y. Ha, Appl. Catal. B: Environ. 84 (2008) 773–782.
[5] H.F. Oetjen, V.M. Schmidt, U. Stimming, F. Trila, J. Electrochem. Soc. 143 (1996) 3838.
[6] A.A. El-Shafei, M. Eiswirth, Surf. Sci. 604 (2010) 862.
[7] A. Ghumman, C. Vink, O. Yepez, P.G. Pickup, J. Power Sources 177 (2008) 71–76.
[8] D.R.M. Godoi, J. Perez, H.M. Villullas, J. Power Sources 195 (2010) 3394–3401.
[9] Q.L. Kang, W.B. Ma, J.J. Wu, M. Pan, Catal. Commun. 10 (2009) 1271–1274.
[10] J.X. Wang, H. Inada, L.J. Wu, Y.M. Zhu, Y.M. Choi, P. Liu, W.P. Zhou, R.R. Adzic, J. Am. Chem. Soc. 131 (2009) 17298–17302.
[11] Z. Liu, J.E. Hu, Q. Wang, K. Gaskell, A.I. Frenkel, G.S. Jackson, B. Eichhorn, J. Am. Chem. Soc. 131 (2009) 6924–6925.
[12] Y. Zhao, X. Yang, J. Tian, F. Wang, L. Zhan, Int. J. Hydrogen Energy 35 (2010) 3249–3257.
[13] C.J. Zhong, L. Luo, P.N. Njoki, D. Mott, B. Wanjala, R. Loukrakpam, S. Lim, L.Y. Wang, B. Fang, Z.C. Xu, Energy Environ. Sci. 1 (2008) 454–466.
[14] G. Chen, D.G. Xia, Z.R. Nie, Z.Y. Wang, L. Wang, L. Zhang, J.J. Zhang, Chem. Mater. 19 (2007) 1840–1844.
[15] S.J. Teng, X.X. Wang, B.Y. Xia, J.N. Wang, J. Power Sources 195 (2010) 1065–1070.
[16] S.T. Nguyen, H.M. Law, H.T. Nguyen, N. Kristian, S.Y. Wang, S.H. Chan, X. Wang, Appl. Catal. B: Environ. 91 (2009) 507–515.
[17] C. Xu, L. Cheng, P. Shen, Y. Liu, Electrochem. Commun. 9 (2007) 997–1001.
[18] C.W. Xu, H. Wang, P.K. Shen, S.P. Jiang, Adv. Mater. 19 (2007) 4256–4259.
[19] S.J. Guo, S.J. Dong, E.K. Wang, Chem. Commun. 46 (2010) 1869–1871.
[20] T.J. Schmidt, H.A. Gasteiger, G.D. Staeb, P.M. Urban, D.M. Kolb, R.J. Behm, J. Electrochem. Soc. 145 (1998) 2354–2358.
[21] K.W. Park, J.H. Choi, B.K. Kwon, S.A. Lee, Y.E. Sung, H.Y. Ha, S.A. Hong, H.S. Kim, A. Wieckowski, J. Phys. Chem. B 106 (2002) 1869–1877.
[22] C. Bock, C. Paquet, M. Couillard, G.A. Botton, B.R. MacDougall, J. Am. Chem. Soc. 126 (2004) 8028–8034.
[23] F. Alcaide, G. Álvarez, P.L. Cabot, O. Miguel, A. Querejeta, Int. J. Hydrogen Energy 35 (2010) 11634–11641.
[24] V. Radmilovic, H.A. Gasteiger, P.N. Ross, J. Catal. 154 (1995) 98–106.
[25] Y.Y. Mu, H.P. Liang, J.S. Hu, L. Jiang, L.J. Wan, J. Phys. Chem. B 109 (2005) 22212–22216.
[26] Y.L. Hsin, K.C. Hwang, C.T. Yeh, J. Am. Chem. Soc. 129 (2007) 999–10010.
[27] M. Chen, Z.B. Wang, Y. Ding, G.P. Yin, Electrochem. Commun. 10 (2008) 443–446.
[28] Z.L. Liu, X.Y. Ling, X.D. Su, J.Y. Lee, J. Phys. Chem. B 108 (2008) 8234–8240.
[29] S. Ha, R. Larsen, R.I. Masel, J. Power Sources 144 (2005) 28–34.
[30] L. Xiao, L. Zhuang, Y. Liu, J. Lu, H.D. Abruña, J. Am.Chem. Soc. 131 (2009) 602–608.
[31] W. Zhang, R. Wang, H. Wang, Z. Lei, Fuel Cells 10 (2010) 34–740.
[32] S. Zhang, Y.Y. Shao, G.P. Yin, Y.H. Lin, Angew. Chem. Int. Edit. 49 (2010) 2211–2214.
[33] B. Liu, H.Y. Li, L. Die, X.H. Zhang, Z. Fan, J.H. Chen, J. Power Sources 186 (2009) 62–66.